Biophysical Chemistry 20 (1984) 285–298
Elsevier

BPC 00884

AN ION-SITE INTERACTION MODEL FOR SODIUM CURRENTS IN THE GIANT AXON

M. COHEN-ARMON *

Department of Physiology and Biophysics, Faculty of Medicine, Technion-Israel Institute of Technology, P.O. Box 9649, 31096 Haifa, Israel

Received 8th November 1983
Revised manuscript received 15th May 1984
Accepted 10th June 1984

Key words: Giant axon; Voltage clamp; Excitability; Nerve membrane; Cooperativity; Na^+ channel

The time and voltage dependence of sodium currents in the *Myxicola* giant axon were examined as functions of the external sodium concentration. The results were incompatible with a model of free diffusion through a gated channel, but lent themselves to analysis in terms of a model involving a positive cooperative homotropic reaction in which Na^+ interacts with two allosteric sites – a regulatory site and a transfer site – at the 'sodium channel'. The time-dependent solution of the rate equations describing the kinetics of the transfer reaction was derived as an expression describing the sodium current as a function of time, membrane potential and external sodium concentration. This function was used to test the validity of the model by its ability to predict the nerve excitability properties. The predicted *i-v* and *i-t* curves fitted the experimental results ($p < 0.005$ and $p < 0.05$, respectively). The computed parameters of these functions are consistent with other experimental results. The possibility of a noncooperative reaction was rejected.

1. Introduction

Experimental evidence incompatible with the notion that the membrane ionic currents can be described in terms of the laws of electrodiffusion is continuously accumulating. This evidence includes: the tendency of ionic currents to saturate as the concentration of permeant ions is raised [1,2], the dependence of sodium permeability on external sodium concentration [3], the attenuation of sodium currents in 'open channels' by other cations [4,5], the dependence of the ionic selectivity on internal or external ion concentration [6,7], the deviation of the reversal potential from the Goldman-Hodgkin-Katz equation predictions [8], and the effect of neurotoxins, which stabilize gates at the open state, on the ionic selectivity in neuroblastoma membrane [9].

To account for these findings, various modifications of the free electrodiffusion model, as well as some new models, were proposed. In essence, these models incorporate ion transfer through 'channels' with fixed energy barriers. The early models for 'Na^+ transfer' were based on the 'single ion pore' model [1,10–12]. Although successfully describing many of the membrane permeability properties, the single ion restriction was subsequently removed [6] to account for ion flux coupling [1,13,14], as well as for the asymmetric nature of the concentration dependence of ion selectivity [2]. Furthermore, there is evidence pointing towards sodium current control by allosteric interactions in the 'open sodium pore' in the giant axon [15–17] and in neuroblastoma cells [9].

This presentation attempts to describe the gating mechanism and the open pore properties [1,18] as dependent entities of a transfer process in the

* Present address: Department of Biochemistry, George S. Wise Faculty of Life Sciences, Tel-Aviv University, 69978 Ramat-Aviv, Israel.

sodium channel involving a voltage dependent, positive, cooperative reaction, Na^+ being the positive effector and the substrate. The validity of this model is tested by comparing the experimental sodium current as a function of time, membrane potential and Na^+ concentration in the external solution with the model's predictions.

2. Materials and methods

Myxicola giant axons were dissected and mounted, as described by Goldman and Binstock [19], and voltage-clamped using the methodology described by Adelman et al. [20]. Series resistance error was partly compensated for on-line [21], while the remaining error was corrected analytically off-line [22]. The axons were externally perfused by artificial seawater (ASW) solutions containing various sodium concentrations (the normal sodium concentration in ASW is 0.43 M). Osmolarity was maintained by substituting Tris for Na^+. Temperature was held at $5 \pm 1°C$.

A minicomputer system generated the command potentials, and controlled the sampling of currents [22]. Holding potential values equal the resting potential. The mean value of the resting potential was -65 mV. Pairs of pulses were given to axons at 15-s intervals. Each pair consisted of a 50 ms hyperpolarizing prepulse to -65 mV (relative to resting potential) and a 12 ms depolarizing test pulse, in the range $+40$ to $+100$ mV. The currents were sampled at 100 kHz and were low-pass filtered by the running (three points) average method [23], and corrected for baseline shifts and leakage [22]. Sodium currents were obtained by subtracting potassium currents (measured in ASW containing 300 mM tetrodotoxin (TTX)) from the total membrane currents.

Model parameters were optimized to fit the experimental results (average from 30 preparations) using a nonlinear, least mean-square technique [24].

3. The model

The effect of external sodium concentration on sodium currents is analyzed in terms of a model consisting of a homotropic cooperative reaction where Na^+ is both the substrate and a positive effector. The reaction is assumed to involve two allosteric sites, a 'regulatory' and a 'transfer' site which are parts of an assumed channel component. This two-sites component is designated as E_0 or E_0^* (see the reaction scheme in fig. 1A) according to whether the regulatory site is activated or inactivated, respectively.

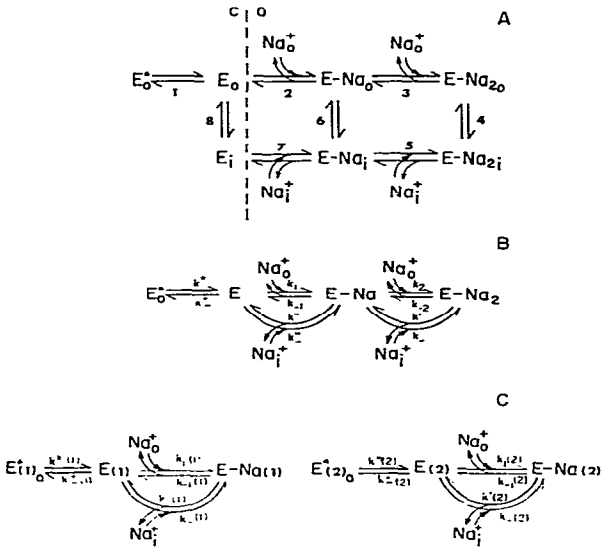

Fig. 1. (A) A cooperative reaction scheme for sodium transfer through the ionic channel. 0 and i, outer and inner sides of the membrane, respectively. E_0^*, inactivated component E consisting of two allosteric Na^+ binding sites; E_0, activated component E; E-NA, $E\text{-}Na_2$ regulatory site and both regulatory and transfer sites, respectively, occupied by Na^+. C and O, closed and open sodium channel states. (B) The simplified scheme of the cooperative transfer reaction. k_1, k_{-1} and k_2, k_{-2}, reaction rate constants of Na^+ binding with the regulatory and transfer sites, respectively, in the external part of the ionic channel; k'', k''_- and k', k_-, reaction rate constants for Na^+ binding in the internal part of the 'channel'. k^*, k^*_-, reaction rate constants of the voltage-dependent activation of E_0^*. (C) A non-cooperative transfer reaction scheme. E(1), E(2), two activated nonallosteric sodium-binding sites, $E\text{-}Na^{(1)}$, $E\text{-}Na^{(2)}$, activated components occupied by Na^+; k_1, k_{-1} and k', k_-, reaction rate constants of each reaction (subscripts (1) or (2)) for Na^+ binding in the external and internal parts of the ionic channel, respectively. k^*, k (subscripts (1) or (2)), reaction rate constants of the voltage-dependent activation of E*(1) and E*(2), respectively ([E*](1), [E*](2), inactivated nonallosteric sodium-binding sites.).

According to the model, following an increase in the membrane potential, the inactivated regulatory site becomes available mainly to external Na^+ (step 1 in the reaction scheme, fig. 1A). This is assumed to be part of the traditional gating process. The subsequent binding of Na^+ to this site causes, by an allosteric effect, an increased affinity of the transfer site to bind Na^+ from both internal and external solutions. This capacity to interact with Na^+ in both solutions is attributed to voltage-dependent, conformational rearrangements in the active component E between states available to Na^+ in the external solution (state O) and in the internal solution (state i) (Fig. 1A). Thus, the transfer process follows the mechanism of transfer by a carrier [25], and the kinetics of a voltage-dependent enzymatic reaction. In the reaction scheme given in Fig. 1A, E_o^*, E-Na, and $E\text{-}Na_2$ denote the component with an inactivated regulatory site, that with an activated regulatory site occupied by an Na^+, and that with both regulatory and transfer sites occupied by Na^+, respectively. The subscripts o and i refer to complexes at the external and internal membrane surfaces, respectively. According to the model, the transfer process is associated mainly with the transformation of $E\text{-}Na_2(o)$ to E-Na(i) and vice versa (i.e., $E\text{-}Na_2(i)$ to E-Na(o)).

In view of the lack of information regarding transformations within the membrane, steps 4–6 and 6–8 (see fig. 1A) are merged to give the simplified scheme presented in fig. 1B.

This scheme will be the basis for the fitting of the model with the experimental data. In this reaction scheme, k_1 and k_{-1} denote the rate constants of the regulatory reaction, k_2 and k_{-2} those of the transfer reaction, k_- and k''_- the overall rate constants of Na_i^+ binding to the transfer and regulatory sites, respectively; and k' and k'' denote the rate constants for Na^+ release from these sites to the inner solution. Thus, the curved arrows define the reactions within, or at the inner surface of the membane. k^* and k^*_- denote the rate constants of the voltage-dependent activation of the regulatory site. These rate constants are assumed to take finite values only during a change in membrane potential. Under a constant membrane potential (voltage clamp conditions) k^* and k^*_- are assumed to be equal to zero. The membrane potential dependence of the ion-transfer rate is assumed to follow the Eyring theory [26]. Linearity has been assumed for the dependence of the free energy on the electric potential for each step of the transfer reaction. The linearity factor (δ) was determined numerically by fitting the computed and experimental data.

The voltage dependence of the reaction rate constants is defined as follows:

$$k_1 = \bar{k}_1 \exp(\delta_1 V) \tag{1}$$

$$k_2 = \bar{k}_2 \exp(\delta_2 V) \tag{2}$$

$$k' = \bar{k}' \exp(-\delta_3 V) \tag{3}$$

$$k'' = \bar{k}'' \exp(-\delta_4 V) \tag{4}$$

where $V = (zF/RT)E_m$, $\bar{k}_{-1}$, $\bar{k}_{-2}$, $\bar{k}_-$ and $\bar{k}''_-$ have the analogue expression except for the change of sign in the exponents. The bars denote rate constants independent of membrane potential.

These definitions follow the assumption that the affinity of the site for Na^+ increases when the membrane potential becomes more positive. The voltage dependence of the rate constants of the reactions in the inner and outer membrane surfaces (δ_3, δ_4 and δ_1, δ_2, respectively) was assumed to be different, while at each surface it was assumed to be equal for both regulatory (δ_1, δ_4) and transfer (δ_2, δ_3) reactions.

In analogy to allosteric interactions in protein molecules participating in cooperative enzymatic reactions, the proposed reaction is assumed to be controlled by conformational rearrangements induced both by the membrane electrical field and by the binding of Na^+ to specific sites in the ionic channel. Also, in analogy to the process in a 'single ionic channel' [27], the transfer reaction intermediaries denoted to the right of the interrupted vertical line in fig. 1A corespond to an open channel state, whereas those to the left correspond to a closed state. The intermediary E-Na represents an open channel state, since according to the assumed allosteric effect, ions that bind to E-Na, an occupied regulatory site, can be transferred through the ionic channel.

Sodium currents at various membrane potentials and sodium concentrations will be described

by the kinetics of the cooperative transfer reaction under the following assumptions: (1) The flow of sodium current, in the voltage and space-clamped membrane, does not involve an ion concentration change in the membrane. The changes in Na^+ concentration on both sides of the membrane are due exclusively to the transfer of the ions through the membrane. Thus, for sodium current, the Na^+ concentration change in the internal solution, $[\dot{N}a_i^+]$, is given by [15]:

$$[\dot{N}a_i^+] = (-4/(Fd))I_{Na} \equiv fI_{Na} \tag{5}$$

where F is Faraday's constant, d the axon diameter and I_{Na} sodium current density. The square brackets are used to denote molar concentration, and the overriding dot denotes the first derivative, throughout. It is easy to show that the factor (f) relating $[\dot{N}a_i^+]$ to I_{Na} is such that, for an axon 400 μm in diameter, an internal sodium concentration change of 1 mM/s is equivalent to a sodium current density of 1 mA/cm^2. (2) The membrane may be considered homogeneously charged (low ionic channel density), and the ionic solutions near the membrane homogeneous (this assumption implies constant ionic strength and no ionic binding). Thus, the ionic concentrations near the membrane are linearly related to the bulk concentrations, according to the Boltzman distribution. (3) Under constant surface potentials ('fixed charges' on the membrane matrix [28]), the linearity factor relating sodium concentration near the membrane and in the bulk solutions remains the same for different membrane potentials.

According to the model, the time-dependent solution of the transfer-reaction rate equations defines the time, membrane potential and $[Na^+]$ dependence of the membrane sodium currents. The rate equations according to the reaction scheme presented in fig. 1B and eq. 5 are:

$$[\text{E-}\dot{N}a_2] = -(k_{-2} + k')[\text{E-Na}_2] + (k_2[Na_0^+] + k_-[Na_i^+])[\text{E-Na}] \tag{6}$$

$$[\text{E-}\dot{N}a] = (k_{-2} + k')[\text{E-Na}_2] - (k_{-1} + k_2[Na_0^+] + k_-[Na_i^+] + k'')[\text{E-Na}] + (k_1[Na_0^+] + k_-''[Na_i^+])[\text{E}] \tag{7}$$

$$[\dot{\text{E}}] = (k_{-1} + k'')[\text{E-Na}] - (k_1[Na_0^+] + k_-''[Na_i^+] + k_-^*)[\text{E}] + k^*[\text{E}_0^*] \tag{8}$$

$$I_{Na} = f^{-1}[\dot{N}a_i] = f^{-1}\{k'[\text{E-Na}_2] + (k'' - k_-[Na_i^+])[\text{E-Na}] - k''[Na_i^+][\text{E}]\} \tag{9}$$

$$E_{tot} = [\text{E}] + [\text{E-Na}] + [\text{E-Na}_2] + [\text{E}_0^*] \tag{10}$$

The concentration of inactivated sites E_0^* was assumed to be constant under voltage clamp conditions, as k^* and k_-^* were assumed to equal zero under a constant membrane potential. Under these conditions eq. 8 becomes redundant. Also, $[E_0^*]$ is assumed to be negligibly small at the depolarization potentials used. The full sequence of the solution of the rate equations is given in the appendix.

Substitution of the time-dependent solution to eqs. 6–10, i.e., the functions $[\text{E-Na}]_t$ and $[\text{E-Na}_2]_t$, in eq. A5 yields an expression for sodium current as a function of time, membrane potential and sodium concentration in the solution near the membrane:

$$\begin{aligned} I_{Na} = f^{-1}C_1\{&(k' + k_-''[Na_i^+])a_{12}/(a_{11} + \lambda_1) \\ &\times (\exp(\lambda_1 t) - \lambda_1/\lambda_2 \exp(\lambda_2 t) \\ &- (\lambda_2 - \lambda_1)/\lambda_2) + (k'' + k_-''[Na_i^+] \\ &- k_-[Na_i^+])(\exp(\lambda_1 t) \\ &- \lambda_1/\lambda_2(a_{11} + \lambda_2)/(a_{11} + \lambda_1)\exp(\lambda_2 t) \\ &+ (\lambda_1 - \lambda_2)a_{11}/(\lambda_2(a_{11} + \lambda_1)))\} \\ &- k_-''[Na_i^+](E_{tot} - [\text{E}_0^*]) \end{aligned} \tag{11}$$

where λ_1 and λ_2 are the inverse values of the system's relaxation times and C_1 an integration constant (determined in the appendix).

An expression for the peak sodium current vs. membrane potential (i-v curves) is obtained by inserting a zero value for the first derivative of the expression for I_{Na} vs. t (eq. A5).

$$I_{Na_{peak}} = f^{-1}((k' + k_-''[Na_i^+])[\text{E-}\dot{N}a_2] - (k_-[Na_i^+] - k'' - k_-''[Na_i^+])[\text{E-}\dot{N}a])/$$

$$(k_- - k''_-)[\text{E-Na}] - k''_-[\text{E-Na}_2] + k''_-(E_{tot} - [\text{E}^*_0])) \quad (12)$$

Eqs. 11 and 12 * were used to reproduce the experimentally defined characteristics of the relations: I_{Na} vs. t and peak I_{Na} vs. v (i-v curves), respectively.

For comparison, an additional model was tested, which evolves two nonallosteric binding sites in the 'Na^+ channel' (E(1), E(2)) (see fig. 1C). In analogy to the model in fig. 1B, $k'(1)$, $k_-(1)$ and $k'(2)$, $k_-(2)$ denote rate constants in the inner interface of the membrane. $k_1(1)$, $k_{-1}(1)$ and $k_1(2)$, $k_{-1}(2)$ denote rate constants of the reactions in the outer interface of the membrane. k^*, k^*_- denote rate constants of the voltage-dependent activation process of components E*(1) and E*(2). The expression for peak sodium current vs. membrane potential (i-v curve) according to the reaction scheme in fig. 1C is:

$$I_{Na_{peak}} = f^{-1}\{(k'(1)[\text{E-Na}](1) + k'(2)[\text{E-Na}](2)) - (k_-(1)[\dot{\text{E}}](1) + k_-(2)[\dot{\text{E}}](2))[Na_i^+]/(k_-(1)[\text{E}](1) + k_-(2)[\text{E}](2))\} \quad (14)$$

4. Experimental

4.1. Sodium i-v curves

A comparison between the experimental and computed peak current vs. membrane potential (i-v curves) at various sodium concentrations is presented in fig. 2. The computed values were obtained using eq. 12, into which the voltage-dependent rate constants were inserted according to eqs. 1–4 (for the full derivation see appendix). The curves represent the computed values, which gave the best fit with the experimental data as obtained by using a nonlinear least-mean-square technique * (see section 2). The measured peak sodium current densities (symbols) are averages from 30 preparations.

Table 1 lists the computed parameters evaluated from the fit of the model with the experimental data. The χ^2 test was used to evaluate the fit of the experimental i-v curves with those predicted by the model (eqs. 12 and 13). The fit is very good ($p < 0.005$). The relations between the computed

* See footnote, this page, column 1.

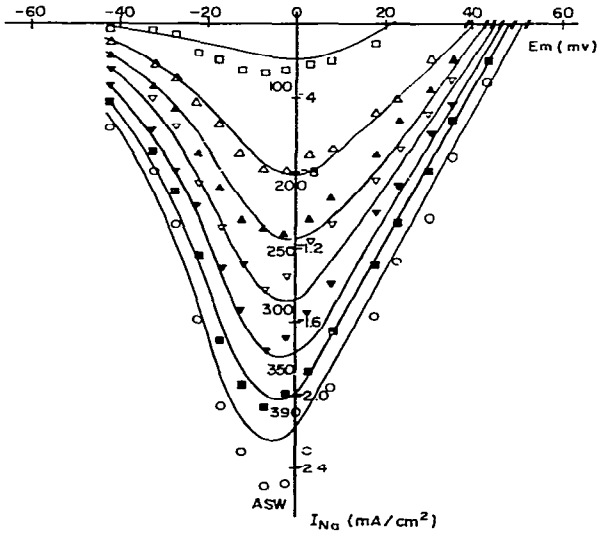

Fig. 2. Peak sodium current density (mA/cm²) as a function of membrane potential (mV) (i-v curves) at various external sodium concentrations (mM) (indicated by each curve). Experimental values obtained in different Na_0^+ concentrations are denoted by different symbols (430(○), 390(■), 350 (▼), 300(▽), 250(▲), 200(△), 100(□)). Each value presents an average from 30 axons. The solid curves were computed on the basis of a cooperative reaction kinetics (fig. 1B) according to eq. 12. The extrapolated experimental reversal potentials are indicated on the v-axis (see text).

* The fitting procedure was done in two stages, in order to work with a minimal number of unknown parameters. In the first stage, an alternative derivation for the peak I_{Na} vs. v function has been used (eq. 13), under the approximation of steady-state condition at the peak sodium current ($\dot{I}_{Na} = 0$). This approximation is reasonable during small depolarizations when the reverse reaction rate is very small (see eqs. 1–4 and 12).

$$I^1_{Na_{peak}} = f^{-1}\{E_{tot} - [\text{E}^*_0])(k' + k''_-[Na_i^+] - (k_-[Na_i^+] - k'' - k''_-[Na_i^+])(k' + k_{-2}) / (k_2[Na_0^+] + k_-[Na_i^+])) / ((k' + k_{-2}) / (k_2[Na_0^+] + k_-[Na_i^+]) + (k_{-2} + k')(k_{-1} + k'') / ((k_2[Na_0^+] + k_-[Na_i^+])(k_1[Na_0^+] + k''_-[Na_i^+])) + 1) - k''_-[Na_i^+](E_{tot} - [\text{E}^*_0]) \quad (13)$$

Table 1

The calculated parameters for the cooperative model (fig. 1B) derived from sodium i-v curves according to eqs. 12 and 13

		$\nu = 89$ $\chi^2 = 23.6$	
$\bar{k}'E_{tot} = (2.12 \pm 0.27)^2 \times 10^{-3}$	$\bar{k}_{-1}/\bar{k}_1 = (0.68 \pm 0.06)^2$	$\bar{k}_{-2}/\bar{k}_2 = 0.08 \pm 5.0 \times 10^{-3}$	$\bar{k}''E_{tot} = (0.2 \pm 0.01)^2 \times 10^{-3}$
$\bar{k}_- E_{tot} = (6.6 \pm 0.85)^2 \times 10^{-3}$	$\delta_1 = \delta_2 = (0.78 \pm 0.04)^2$	$\bar{k}_2 = (2.8 \pm 0.1) \times 10^3$	$\bar{k}''_- E_{tot} = (0.25 \pm 0.01)^2 \times 10^{-3}$

The parameters were obtained for the best fit (minimal χ^2 value) of the experimental to computed results, using a nonlinear regression method [24]. ν defines the number of degrees of freedom, k_{-1}, k_1 denote the rate constants for Na_0^+ dissociation (s^{-1}) and binding ((s mol)$^{-1}$) in the regulatory reaction, at 0 mV; k_{-2}, k_2 denote these rate constants in the transfer reaction; k', k_- denote the rate constants for Na_i^+ dissociation and binding, repectively, in the transfer reaction; k'', k''_- denote these rate constants in the regulatory reaction; E_{tot} (M) denotes total concentration of active sites. The parameters are represented by the squares of the values ± S.D. (details are given in the text). δ_1 and δ_2 (defined in eqs. 1 and 2); δ_3 and δ_4 (defined in eqs. 3 and 4) are equal to 1.0 throughout the calculations.

values of the rate constants are consistent with the characteristics of a cooperative mechanism, i.e., the affinity of the transfer site (k_2/k_{-2}) is an order of magnitude larger than that of the regulatory site (k_1/k_{-1}). The rate constant of inward Na^+ release from the regulatory site (k'') is smaller by two orders of magnitude compared with that from the transfer site (k'). The value of the ratio k_{-1}/k_1 is also close to the normal Na^+ concentration in ASW, as would be expected if such a mechanism operates under physiological conditions [29]. Also, the values of the rate constants of the transfer reaction (k_{-2} and k_2) are compatible with the mean open time of a single channel determined from patch-clamp analysis [27].

The experimental data illustrated in fig. 2 are redrawn in figs. 3 and 5 to display I_{Na} as a function of $[Na_0^+]$ (in analogy with a reaction rate vs. the substrate concentration) at various potentials (indicated by different symbols for the different membrane potentials). The experimental data show relationships which are compatible with cooperative kinetics. However, the S-shaped relationship typical of cooperative kinetics is not evident, as the concentration of isotonic Na^+ is not sufficiently high to reach saturation. The curves approach saturation only at hypertonic concentrations, as illustrated in fig. 4, which depicts, for the computed values of $I_{Na_{peak}}$ vs. $[Na_0^+]$, a wider Na_0^+ concentration range ($\approx$ 3.5-times the normal Na^+ concentration in ASW). With increasing membrane potential, saturation is reached at lower Na_0^+ concentration, and the degree of cooperativity is increased as expressed by the slopes of the curves in figs. 3 and 4 [29]. For the computed data in figs. 3 and 4 this evolves from the assumption that the affinity of the active sites to Na^+ increases with increasing membrane potential (eqs. 1–4).

The same analysis was carried out on the experimental data assuming a reaction mechanism which involves two nonallosteric sites (reaction scheme in fig. 1C) according to eq. 14. The curves in fig. 5 represent the computed values, which gave the best fit with the experimental data. The fit is

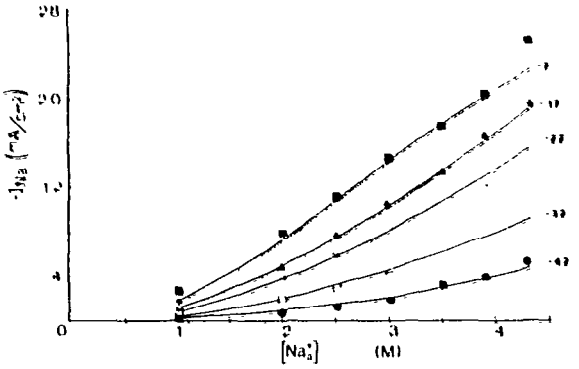

Fig. 3. Peak sodium current density as a function of external sodium concentration, at various membrane potentials. The experimental values (same as in fig. 2) are denoted by different symbols for each membrane potential (indicated by each curve −7 mV (■), −17 mV (▲), −22 mV(△), −32 mV(□), −42 mV(●)). The curves were computed on the basis of cooperative reaction kinetics (fig. 1B) according to eq. 12 (see text).

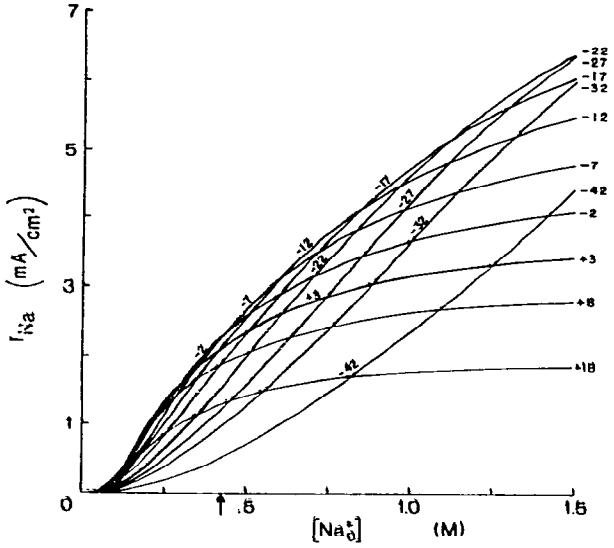

Fig. 4. Computed values of peak sodium current density, as a function of sodium concentration in the external solution in the range 0.05–1.5 M, for different membrane potentials indicated by each curve (mV). The current values were computed on the basis of a cooperative reaction kinetics (fig. 1B) according to eq. 12 (see text). The arrow indicates sodium concentration in ASW.

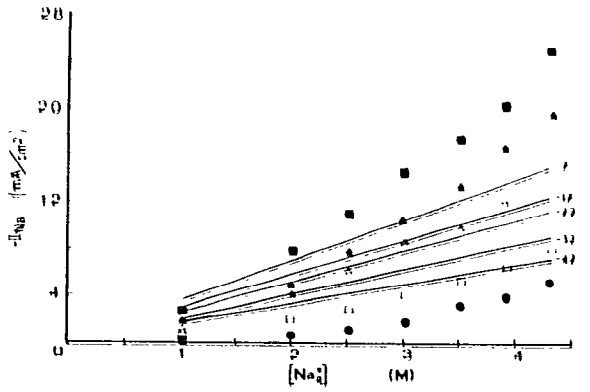

Fig. 5. Peak sodium current density as a function of external sodium concentrations, at various membrane potentials. The experimental values (same as in fig. 3) are denoted by different symbols for each membrane potential (indicated by each curve (mV)). The curves were computed on the basis of a noncooperative reaction kinetics (fig. 1C), according to eq. 14 (see text).

very poor (χ^2 corresponds to $0.75 < p < 0.9$). Thus, the experimental results are incompatible with this model. Similar incompatibility was obtained for an assumed reaction involving one binding site.

Two more characteristics of the sodium *i-v* curve were derived according to the model (fig. 1B):

4.1.1. The reversal potential

The predicted intercept of the *i-v* curve (according to eq. 12 with the *v*-axis ($i_{Na} = 0$) should be the reversal potential (E_{Na}).

The reversal potential is generally defined as the potential at which the net current equals zero at any time. According to the model, the expression for E_{Na} was derived by setting zero net sodium current in eq. 9 * and the expressions for $[E\text{-}Na]_{t\to\infty}$ and $[E\text{-}Na_2]_{t\to\infty}$ (eqs. A10 and A11). The expression obtained from eq. 9 * is:

$$(k_2[Na_0^+] + k_-[Na_i^+])/(k_{-2} + k') = k_-[Na_i^+]/k' \qquad (15)$$

By inserting the voltage-dependent relationships of the rate constants (eqs. 1–4) into eq. 15, the expression obtained for the *i-v* curve intercept with the *v*-axis is:

$$E_{Na} = (2(\delta_1 = \delta_2))^{-1} RT/zF\{\ln(\bar{k}\ \bar{k}_{-2}/\bar{k}'\bar{k}_2) + \ln([Na_0^+]/[Na_i^+])\} \qquad (16)$$

After inserting the values of δ_2 and δ_1 and the rate constants at zero potential (see table 1) in eq. 16, the expression for the predicted E_{Na} was obtained. For an external sodium concentration of 0.43 M the predicted E_{Na} was 0.98–1.25-times the Nernst potential. For an external sodium concentration of 0.2 M, the predicted E_{Na} was 0.8–1.03-times the Nernst potential. Thus, the predicted *i-v* curve intercept approximately equals the Nernst equilibrium potential value [1,30–32]. The experimental E_{Na} values were evaluated by linear extrapolation from the measured sodium currents near these potentials (fig. 2). The predicted E_{Na} values fit with the experimental values for the various external Na^+ concentrations (see Fig. 2).

* $\bar{k}''$, $\bar{k}_-''$, which are negligibly small relative to $\bar{k}'$, $\bar{k}_-$ (see table 1), have been neglected for the sake of simplicity.

4.1.2. The instantaneous i-v curves

The instantaneous *i-v* curve characteristics may be reproduced according to the model using the expression for sodium current vs. time (eq. A5 *), and the boundary condition at $t = 0$ (eqs. A6 and A7), which exists during the instantaneous potential step, as long as λ_1, λ_2 are sufficiently large (eq. 11). This is subsequently shown (see p. 294). Following the incorporation of this condition into eq. A5, an expression for the slope of the instantaneous sodium *i-v* curve is obtained:

$$\begin{aligned}(I_{Na_{E_1}} - I_{Na_{E_2}})/(E_1 - E_2) &= f^{-1}\{[\text{E-Na}_2]_{E_0}\bar{k}'(\exp(-\delta_3 XE_1) \\ &\quad - \exp(-\delta_3 XE_2)) \\ &\quad + [\text{E-Na}]_{E_0}\bar{k}_-[\text{Na}_i^+](\exp(\delta_3 XE_2) \\ &\quad - \exp(\delta_3 XE_1))\}/(E_1 - E_2) \qquad (17)\end{aligned}$$

where $X = zF/RT$, E_1 and E_2 are membrane potentials after the instantaneous potential change, and E_0 the membrane potential preceding the potential step. After expanding the exponents in eq. 17 into Maclaurin's series, and using the first two terms in the series, the following expression for the slope of the instantaneous *i-v* curve is obtained:

$$\begin{aligned}dI/dE = -f^{-1}(&\bar{k}'[\text{E-Na}_2]_{E_0} \\ &+ \bar{k}_-[\text{Na}_i^+][\text{E-Na}]_{E_0})(zF/RT)\delta_3 \qquad (18)\end{aligned}$$

Thus, the chord conductance seems, according to eq. 18, to be independent of the instantaneous 'post' potentials E_1 and E_2 for small values of membrane potentials (in the range of approx. ± 20 mV), and to be dependent only on the potential preceding the instantaneous step, as was experimentally determined for a reasonably wide potential range [33,34].

4.2. Sodium i-t curves

The time-dependent solution of the reaction-rate equations (eqs. 6–10) yields an expression for sodium current vs. time, membrane potential and sodium concentration in the external and internal media (eq. 11). Most of the reaction rate constants in eq. 11 were obtained from the optimal fit of the computed to experimental sodium *i-v* curves (using eqs. 12 and 13), as described in section 4.1, and inserted in eq. 11, in order to establish the fit of experimental with computed currents vs. time. Two additional parameters, the regulatory reaction-rate constant (k_1) and the total concentration of active sites (E_{tot}) were required to enable the complete description of the time dependence of the currents by the model. These parameters were calculated for two sodium concentrations by fitting the experimental curves to the predicted ones (eq. 11) (table 2). Fig. 6 presents the fitting of computed (solid curves) to experimental (dashed curves) sodium currents. The experimental results seem to be reasonably predicted by the model. The χ^2 goodness-of-fit test was used. $p < 0.005$ was obtained for the lower Na_0^+ concentration (200 mM), $p < 0.05$ was obtained for the data measured in ASW solution (430 mM). The χ^2 values were computed considering both the experimental errors and the computed errors of the parameters calculated from the *i-v* curves (table 1).

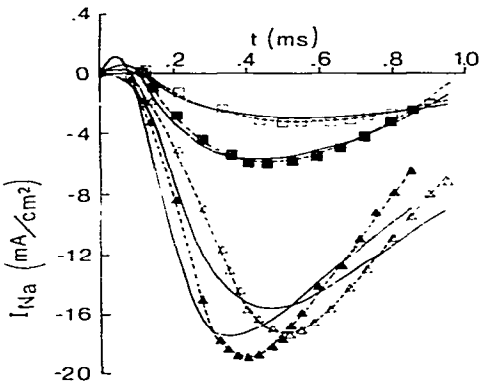

Fig. 6. Sodium current density, experimental (symbols on interrupted lines) and computed (solid curves), as a function of time, at membrane potentials of −20 mV (open symbols) and −10 mV (closed symbols). Sodium concentrations in the external solution are 0.2 M (squares) and 0.43 M (triangles). The computed currents were obtained on the basis of a cooperative reaction kinetics (fig. 1B) according to eq. 11 (measured currents in axon no. ML7728).

* See footnote, p. 291.

Table 2

The calculated parameters for the cooperative model (fig. 1B) derived from sodium *i-t* curves according to eq. 11

	$[Na_0^+] = 0.43$		$[Na_0^+] = 0.2$	
E_m	−20	−10	−20	−10
ν	26	24	21	16
χ^2	14.3	13.7	2.7	2.9
$E_{tot} + \Delta E_{tot}$	$(1.06 \pm 0.08)^2 \times 10^{-5}$	$(0.91 \pm 0.08)^2 \times 10^{-5}$	$(1.44 \pm 0.06)^2 \times 10^{-5}$	$(0.96 \pm 0.07)^2 \times 10^{-5}$
$\bar{k}_1 \pm \Delta \bar{k}_1$	$(1.63 \pm 0.13)^2 \times 10^{4}$	$(1.9 \pm 0.17)^2 \times 10^{4}$	$(1.15 \pm 0.12)^2 \times 10^{4}$	$(1.03 \pm 0.07)^2 \times 10^{4}$

The currents were measured at membrane potentials of −20 and −10 mV. Sodium concentrations in the external solution were 0.2 and 0.43 (mol/l). The parameters were obtained for the best fit (minimal χ^2) of the experimental and computed data by using a nonlinear regression method [24]. ν defines the number of degrees of freedom, $\bar{k}_1$ the value of the regulatory reaction rate constant ($s^{-1}\ M^{-1}$) at 0 mV, and E_{tot}(M) the total concentration of active sites (details are given in the text).

The values of the computed parameters (see tables 1 and 2) are consistent with other experimental results:

(1) The values of the rate constants of the regulatory reaction ($\bar{k}_1$ and $\bar{k}_{-1}$) are compatible with the time constants for 'opening' of sodium channels estimated from gating current analysis [35]. These rate constants are also greater by 4 orders of magnitude than the corresponding rate constants in the inner side of the membrane (k'' and k''_-), which is consistent with the notion that the regulatory site is available mainly to Na^+ in the external solution.

(2) The computed values of the relaxation times $|\bar{\lambda}_1^{-1}|$, $|\bar{\lambda}_2^{-1}|$ at 0 mV, and Na_0^+ concentration of 0.43 M − 0.055×10^{-3} s $< |\bar{\lambda}_1^{-1}| < 0.062 \times 10^{-3}$ s and 0.77×10^{-3} s $< |\bar{\lambda}_2^{-1}| < 0.87 \times 10^{-3}$ s − were obtained by substitution of the computed rate constants into eq. A16, and are of the same order of magnitude as those of the time constants of the onset (m) and decay (h) processes, respectively, of sodium current in the Hodgkin-Huxley axon model. Obviously, $|\lambda_1^{-1}|$ is also compatible with the experimentally estimated time constant of the gating current turn-on [18,35]. The dependence of the relaxation times on external sodium concentration

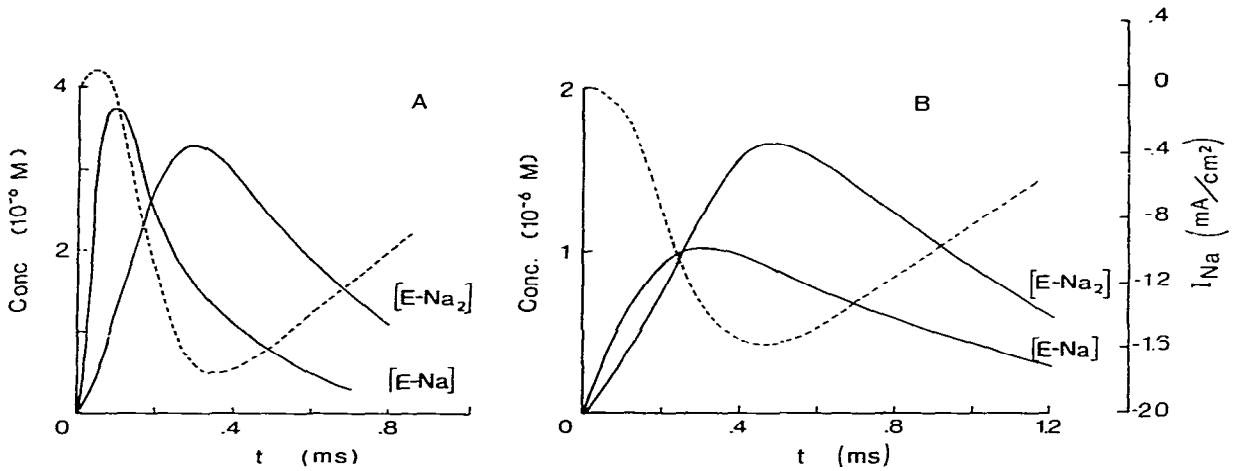

Fig. 7. The time dependence of the concentration of the intermediaries ([E-Na] vs. t. [E-Na_2] vs. t) (defined in the reaction scheme, fig. 1B), and the computed sodium currents (interrupted lines). The curves were computed according to eqs. A10, A11 and A5 (see text) for normal external sodium concentration (ASW) and two membrane potentials: (A) −10 mV, (B) −20 mV.

(eq. A16) quantitatively predicts the dependence of sodium current pattern (I_{Na} vs. t) on Na_0^+ concentration (further discussed on p. 295 and fig. 8).

According to the model, the function describing I_{Na} vs. t (eq. A5) is a linear combination of the intermediaries' concentration ([E-Na] and [E-Na_2]) vs. t functions. Fig. 7 shows the intermediaries' concentration changes and the computed sodium current densities (fig. 6) for two depolarization potentials and for normal Na_0^+ concentration (430 mM). It can be seen that the rising phase of sodium current roughly follows the falling phase of $[E\text{-}Na]_t$, while the decay of the current follows mostly the decay of $[E\text{-}Na_2]_t$. This illustrates the analogy between the intermediary E-Na and the open channel concept.

4.3. Sodium channel density

On the basis of the assumption that protein molecules spanning the phospholipid matrix of the membrane (the model of Singer and Nicholson [36]) construct the ionic channels [37], the sodium channel density can be estimated from the value of E_{tot} according to the model, if E is identified with the sodium channel. Under these assumptions the average total concentration of active sites E_{tot} per unit volume at -10 mV (table 2) was translated into sodium channel density per unit area. The value obtained was approx. 100 channels/μm^2, which is in the range of the predicted values for sodium channel density in the giant axon, obtained in experiments using the inhibitory effect of TTX (324 sites/μm^2 [38]), or gating current analysis (220 sites/μm^2 [39]).

5. Discussion

In the described model, Na^+ is the substrate and a positive effector in the cooperative transfer process of Na^+ through the activated membrane. Within this framework, the membrane-conductance changes associated with excitability are a function of sodium concentration in the external and internal solutions as well as of potential. This is contrary to the 'independence principle' predictions [30], whereby Na^+ is a charge carrier transferred by electrodiffusion through voltage-gated channels.

The proposed model differs from models based on the single-file electrodiffusion description of ionic permeation [1,6,10,11] in the assumption of a variable energy profile in the Na^+ channel. The single-file electrodiffusion models assume a fixed energy profile in the sodium channel. Whereas according to the proposed model, changing sodium concentration in the aqueous phase (and thus the average occupancy of sites E) will change the conformational state of the channel and affect its permeability. This leads to a nonlinear concentration dependence of permeability, different from the simple saturation characteristics predicted for channels with fixed barrier structure. This also leads to a concentration dependence of the onset time of sodium current not predicted by the electrodiffusion model (further discussed on p. 295).

One of the main conclusions that can be reached on the basis of this work is that both the gating process and the open pore states are involved in the transfer reaction. This conclusion is supported by the good fit of the experimental data with both the reconstructed sodium currents vs. time, and the reconstructed i-v curves. The latter represent mainly the voltage dependence of sodium currents in the state of open channels. Further support of the model can be found in: (a) the fact that the computed rate constants of the proposed transfer reaction are compatible with those of the Hodgkin-Huxley model and those obtained from gating currents and 'patch-clamp' analysis, (b) the similarity to the dependence of peak I_{Na} on $[Na^+]_0$ obtained by Takenaka et al. [40] in perfused squid axons, using hypertonic Na_0^+ solutions (up to 3-times the normal Na^+ concentration in ASW).

Cooperative reactions involving structural transformations induced by ion-protein interactions are common in protein chemistry [41,42] (occurring in a time range of picoseconds to seconds [43]). The sodium-transfer reaction described here can be attributed to a cooperative mechanism, where structural changes in the sodium channel are induced by both ion binding and membrane electric field changes. A cooperative mechanism involving two allosteric sites has been

suggested to account for the effect of positive ions in the external solution on the kinetics of sodium transfer through neurotoxin-stabilized open channels in neuroblastoma, and chicken embryonic muscle cell membranes [9,44,45]. Similarly, the blocking effect of low pH on Na^+ conductance in the giant axon is compatible with a model involving an interaction between two allosteric sites located at the opening and the inner part of the Na^+ pore [46–48].

The validity of the described model for the sodium current mechanism was further tested by its additional prediction, that changes in the positive effector concentration (i.e., $[Na_0^+]$) should affect the rate of onset of the sodium current. Within the framework of the model, this effect is quantitatively provided (according to eq. 11) from the dependence of the relaxation times $|\lambda_1^{-1}|$ and $|\lambda_2^{-1}|$ on the external Na^+ concentration (eq. A16).

In accordance with this prediction the effect of sodium concentration in the external solution on the rate of current onset was observed. Fig. 8 illustrates the increase in the measured sodium current onset period as the external Na^+ concentration is reduced. The points represent measured sodium current at different Na_0^+ concentrations. The interrupted curves were predicted according to eq. 11 and the parameters in tables 1 and 2. As can be seen, the effect of $[Na_0^+]$ is qualitatively predicted by the model.

The effect of Na_0^+ concentration on the rate of sodium current onset could be attributed in part to an uncompensated resistance in series with the voltage-clamped membrane [22]. In order to avoid such artifactual results we used both electronic on-line series resistance compensation [21] and a numerical method for series resistance compensation in the data analysis [22] (see section 2). The delay in the current onset at low Na_0^+ concentration (fig. 8) cannot be explained by a series resistance effect [22]. A similar effect of extracellular Na^+ concentrations on the open time of end plate channels has been reported [49].

The observed effects of $[Na_0^+]$ on sodium current are significant at moderate depolarizations, while they can hardly be detected at positive membrane potentials. According to the model, this is explained by the fact that at positive membrane potentials, the 'Na^+-binding sites' are saturated even at low $[Na_0^+]$, because their affinity for Na^+ at positive potentials is high (eqs. 1–4). This predicts that the effect of $[Na_0^+]$ will be less pronounced for outward Na^+ currents than for the inward currents.

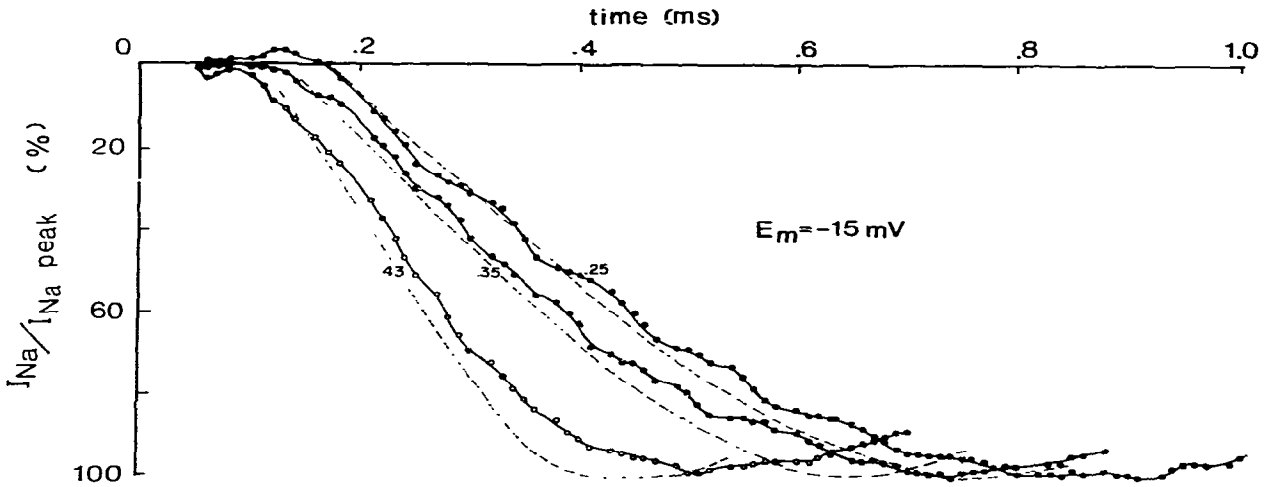

Fig. 8. Sodium current traces (in percentages from the peak currents), at a membrane potential of −15 mV, and various external sodium concentrations (M) indicated as follows: 0.25 (●), 0.35 (◐), 0.43 (○) (currents measured in axon no. ML7783). Computed sodium currents (interrupted lines) according to the model (eq. 11).

Predicted *i-v* curves according to the proposed model including outward sodium currents (eqs. 12 and 13) fit the experimental data of Binstock [50]. Also, predicted outward sodium currents (reconstructed according to eq. 11) have the same pattern observed for outward sodium currents in squid giant axon [51].

In summary, we conclude, on the basis of the compatibility of our experimental results, and of other experimental evidence with the predictions of the presented model hypothesis, that a cooperative reaction of the type described here may be a rate-limiting process in the transfer of Na^+ through the ionic channel.

Appendix

A1. Derivation of the solution of the transfer-reaction rate equations (eqs. 6–9), according to the reaction scheme presented in fig. 1B

Under voltage clamp conditions the rate constants of the voltage dependent activation of E_0^* (k^* and k_-^*) are assumed to equal zero (see section 3). Under these conditions eq. 8 becomes redundant. The set of three nonlinear differential equations (eqs. 6, 7 and 9) may be simplified to a set of two linear differential equations if the internal sodium concentration is treated as constant. Denoting by $[Na_i^+]_t$ its level at time t, and by $[\Delta Na_i^+]_t$ its increment at that time, we have:

$$[Na_i^+]_t = [Na_i^+] + [\Delta Na_i^+]_t \tag{A1}$$

$$[\dot{N}a_i^+]_t = [\dot{N}a_i^+] + [\Delta \dot{N}a_i^+]_t \tag{A2}$$

Assuming that the increment itself is negligible [53], but the rate of change is not, eqs. A1 and A2 become:

$$[Na_i^+]_t \equiv [Na_i^+] \tag{A3}$$

$$[\dot{N}a_i^+]_t \equiv [\Delta \dot{N}a_i^+]_t \tag{A4}$$

Under these conditions, eqs. 6 and 7 are converted into linear differential equations. The following expression is obtained for sodium current at time t:

$$I_{Na} = f^{-1}[\dot{N}a_i^+] = f^{-1}\{(k' + k_-''[Na_i^+])[\text{E-Na}_2] - (k_-[Na_i^+] - k'' - k_-''[Na_i^+])[\text{E-Na}] - k_-''[Na_i^+](E_{tot} - [E_0^*])\} \tag{A5}$$

The boundary conditions for solving eqs. 6, 7, 9 and 10 are:

(i) Continuity of the intermediaries' concentration functions vs. time, namely:

$$[\text{E-Na}]_{t=0, V=V_{n+1}} = [\text{E-Na}]_{t=t_n, V=V_n} \tag{A6}$$

$$[\text{E-Na}_2]_{t=0, V=V_{n+1}} = [\text{E-Na}_2]_{t=t_n, V=V_n} \tag{A7}$$

where t_n is the duration of the nth potential pulse, and V_n and V_{n+1} the amplitudes of two consecutive potential pulses. Under our experimental conditions, $V_n = -65$ mV, $t_n = 50$ ms (see section 2).

(ii) Steady-state conditions are reached over long durations:

$$[\text{E-}\dot{N}a]_{t\to\infty} = 0 \tag{A8}$$

$$[\text{E-}\dot{N}a_2]_{t\to\infty} = 0 \tag{A9}$$

Under these boundary conditions, the initial concentrations of [E-Na] and [E-Na_2] under our experimental conditions, were computed from the rate equations, eqs. 6, 7 and 10, using the definitions in eqs. 1–4. The values obtained for any test pulse were 1.6×10^{-8} and 8×10^{-10} mol/l, respectively *. Under these boundary conditions, the analytical solution of eqs. 6, 7 and 10 reads:

$$[\text{E-Na}]_t = C_1\{\exp(\lambda_1 t) - \lambda_1(a_{11} + \lambda_2)/(\lambda_2(a_{11} + \lambda_1))\exp(\lambda_2 t)\} + (E_{tot} - [E_0^*])(k_1[Na_0^+] + k_-''[Na_i^+])a_{11}/(a_{11}a_{22} - a_{12}a_{21}) \tag{A10}$$

$$[\text{E-Na}_2]_t = C_1\{a_{12}/(a_{11} + \lambda_1)\exp(\lambda_1 t) - \lambda_1 a_{12}/(\lambda_2(a_{11} + \lambda_1))\exp(\lambda_2 t)\} + (E_{tot} - [E_0^*])(k_1[Na_0^+] + k_-''[Na_i^+])a_{12}/(a_{11}a_{22} - a_{12}a_{21}) \tag{A11}$$

* These small values have been substituted by zero, in order to simplify the expressions of the time-dependent solution.

where:

$$a_{11} = k' + k_{-2} \tag{A12}$$

$$a_{12} = k_2[Na_0^+] + k_-[Na_i^+] \tag{A13}$$

$$a_{21} = k_{-2} + k' - k_1[Na_0^+] - k''_-[Na_i^+] \tag{A14}$$

$$a_{22} = k_{-1} + k_2[Na_0^+] + k_-[Na_i^+] + k_1[Na_0^+] + k''_-[Na_i^+] + k'' \tag{A15}$$

$$\lambda_{1,2} = \left(-(a_{11} + a_{22}) \pm \sqrt{(a_{11} - a_{22})^2 + 4a_{12}a_{21}}\right)/2 \tag{A16}$$

where λ_1 and λ_2 are the characteristic roots of the characteristic equation of the linear system (eqs. 6, 7 and 10), and the reciprocals of the reaction relaxation times [52]. C_1 is an integration constant:

$$C_1 = \{\lambda_2(\lambda_1 + a_{11})/(\lambda_1 - \lambda_2)\}(E_{tot} - [E_0^*]) \times (k_1[Na_0^+] + k''_-[Na_i^+])/(a_{11}a_{22} - a_{12}a_{21}) \tag{A17}$$

Acknowledgements

The author gratefully acknowledges the help and support of Professor Yoram Palti during the course of this research, and his critical reviewing of the manuscript. This study was conducted as part of the requirements for the D.Sc. degree of the author at the Technion-Israel Institute of Technology, in the Faculty of Medicine, Department of Physiology and Biophysics.

References

1 B. Hille, J. Gen. Physiol. 66 (1975) 535.
3 T.B. Begenisich and M.D. Cahalan, in: Membrane transport processes, eds. C.F. Stevens and R.W. Tsien (Raven Press, New York, 1979) p. 11.
3 J. Brismar and B. Frankenhaeuser, J. Physiol. 249 (1975) 549.
4 B. Hille, J. Gen. Physiol. 59 (1972) 637.
5 A.M. Woodhull, J. Gen. Physiol. 61 (1973) 687.
6 T.B. Begenisich and M.D. Cahalan, J. Physiol. 307 (1980) 217.
7 R.J. French and J.B. Wells, J. Gen. Physiol. 70 (1977) 707.
8 G.A. Ebert and L. Goldman, J. Gen. Physiol. 68 (1976) 327.
9 M. Lazdunski, M. Balerna, J. Barhanin, R. Chicheportiche, M. Fosset, C. Frelin, Y. Jacques, A. Lombet and J. Pouyssegur, Ann. N.Y. Acad. Sci. 358 (1980) 169.
10 K. Hechmann, in: Biomembranes, vol. 3, eds. F. Kreuzer and J.G.F. Slegers (Plenum Press, New York, 1972) p. 127.
11 P. Lauger, Biochim. Biophys. Acta 311 (1973) 423.
12 Y.A. Chizmadjev and S.K. Aityan, J. Theor. Biol. 64 (1977) 429.
13 C.M. Armstrong, Q. Rev. Biophys. 7 (1975) 179.
14 T. Begenisich and P. Deweer, Nature 269 (1977) 710.
15 M. Cohen, Y. Palti and W.J. Adelman, Jr. J. Membrane Biol. 24 (1975) 201.
16 M. Cohen and Y. Palti, Isr. J. Med. Sci. 14 (1978) 500.
17 A. Strickholm, Biophys. J. 35 (1981) 677.
18 L. Goldman, Q. Rev. Biophys. 9 (1976) 491.
19 L. Goldman and L. Binstock, J. Physiol. 54 (1969) 741.
20 W.J. Adelman, Jr, Y. Palti and J. Senft, J. Membrane Biol. 13 (1973) 387.
21 L. Binstock, W.J. Adelman, Jr, J.P. Senft and H. Lecar, J. Membrane Biol. 21 (1975) 25.
22 Y. Palti and M. Cohen-Armon, Isr. J. Med. Sci. 18 (1982) 19.
23 R.W. Hamming, Numerical methods for scientists and engineers, 2nd edn. (McGraw-Hill, New York, 1973) p. 567.
24 M.J.D. Powell, Comput. J. 7 (1965) 155.
25 P. Lauger, J. Membrane Biol. 57 (1980) 163.
26 H. Eyring, R. Lumry and J.W. Woodbury, Record. Chem. Prog. 100 (1945) 100.
27 F. Conti and E. Neher, Nature 285 (1980) 140.
28 G. Ehrenstein and D.L. Gilbert, Biophys. J. 15 (1975) 847.
29 H.R. Mahler and E.H. Cordes, Biological chemistry (Harper International Editions, New York, 1966) p. 303.
30 A.L. Hodgkin and A.F. Huxley, J. Physiol. 116 (1952) 449.
31 A.L. Hodgkin and A.F. Huxley, J. Physiol. 177 (1952) 500.
32 L. Goldman and C.L. Schauf, J. Gen. Physiol. 61 (1973) 361.
33 A.L. Hodgkin and A.F. Huxley, J. Physiol. 116 (1952) 473.
34 T. Begenisich, J. Gen. Physiol. 66 (1975) 47.
35 C.M. Armstrong and F. Bezanilla, J. Physiol. 63 (1974) 533.
36 S.J. Singer and L. Nicholson, Science 175 (1972) 720.
37 R. Villegas, G. Villegas, M. Condrescu-Guidi and Z. Suarez-Mata, Ann. N.Y. Acad. Sci. 358 (1980) 183.
38 R.D. Keynes, F. Bezanilla, E. Roja and R.E. Taylor, Phil. Trans. R. Soc. Lond. B270 (1975) 365.
39 E. Levitan, J. Theor. Biol. 85 (1980) 423.
40 T. Takenaka, H. Horie and Y. Saeki, Comp. Biochem. Physiol. 62A (1979) 409.
41 R.H. Haschemeyer and A.R.V. Haschemeyer, Proteins: A guide to study by physical and chemical methods (John Wiley and Sons, New York, 1973) p. 368.
42 C. Tanford, Adv. Protein Chem. 17 (1962) 70.
43 G. Papakostides, G. Zundel and M. Emefried, Biochim. Biophys. Acta 288 (1972) 277.
44 M. Lazdunski, M. Balerna, R. Chicheportiche, M. Fosset, Y. Jacques, A. Lombet, G. Romey and H. Schweitz, in: Advances in cytopharmacology, vol. 3, eds. B. Ceccarelli and F. Clementi (Raven Press, New York, 1979) p. 353.

45 Y. Jacques, G. Romey, M. Fosset and M. Lazdunski, Eur. J. Biochem. 106 (1980) 71.
46 F.J. Sigworth and B.C. Spalding, Nature 283 (1980) 293.
47 G.N. Mozhayeva, A.P. Naumov and Y.A. Negulyaev, Gen. Physiol. Biophys. 1 (1982) 5.
48 G.N. Mozhayeva, A.P. Naumov and Y.A. Negulyaev, Gen. Physiol. Biophys. 1 (1982) 21.
49 K. Takeda, P.H. Barry and P.W. Gage, Proc. R. Soc. Lond. B216 (1982) 225.
50 L. Binstock, J. Gen. Physiol. 68 (1968) 551.
51 F.F. Offner, Biophys. J. 12 (1972) 1583.
52 I.S. Sokolnikov, Mathematics of physics and modern engineering (McGraw-Hill, New York, 1966) p. 148.
53 R.D. Keynes, J. Physiol. 114 (1951) 119.